

Graphical Abstract

Collective sedimentation from ash-clouds: insights from experimental buoyant, particle-laden gravity currents

Paul A. Jarvis, Allan Fries, Jonathan Lemus, Costanza Bonadonna, Amanda Clarke, Irene Manzella, Jeremy Phillips

Highlights

Collective sedimentation from ash-clouds: insights from experimental buoyant, particle-laden gravity currents

Paul A. Jarvis, Allan Fries, Jonathan Lemus, Costanza Bonadonna, Amanda Clarke, Irene Manzella, Jeremy Phillips

- Research highlight 1
- Research highlight 2

Collective sedimentation from ash-clouds: insights from experimental buoyant, particle-laden gravity currents

Paul A. Jarvis^{a,*}, Allan Fries^a, Jonathan Lemus^a, Costanza Bonadonna^a,
Amanda Clarke^b, Irene Manzella^c, Jeremy Phillips^d

^a*Department of Earth Sciences, University of Geneva, Rue des Marichers, Geneva,
1205, Switzerland*

^b*School of Earth and Space Exploration, Arizona State University, ISTB4-BLDG75, 781
E Terrance Mall, Tempe, AZ, 85287-6004, USA*

^c*School of Geography, Earth and Environmental Sciences, University of Plymouth, Drake
Circus, Plymouth, PL4 8AA, UK*

^d*School of Earth Sciences, University of Bristol, Wills Memorial Building, Queens Road,
Bristol, BS8 1RJ, UK*

Abstract

Keywords:

1. Introduction

The volcanic ash produced by explosive volcanic eruptions is an economic and societal hazard. Fine ash which is breathed in can cause respiratory health problems in humans and animals (Kampa and Castanas, 2007; Anderson et al., 2012; WHO, 2013; Baxter and Horwell, 2015). Agriculturally, ash deposits can contaminate human and livestock food and water supplies, as well as cover crops (Cook et al., 1981; Cronin et al., 1998; Wilson et al., 2011; Craig et al., 2016). More generally, ash can cause buildings to collapse and damage electrical power systems (Wilson et al., 2014; Craig et al., 2016). A well-publicised impact is that on the aviation industry, whereby the risk of

*Corresponding author: paul.jarvis@unige.ch

damage to airplane engines can lead to costly shutdowns of airspace (Budd et al., 2011; Elisondo et al., 2016). The mechanisms of ash dispersal and sedimentation therefore need to be understood in order for accurate hazard and risk assessments to be carried out.

Key tools used for hazard assessment are ash dispersal models which aim to simulate the transport of volcanic ash in the atmosphere (Witham et al., 2007; Bonadonna et al., 2012; Folch, 2012). These have been used to produce operational forecasts of ash clouds (Scollo et al., 2009; Webster et al., 2012) or to produce hazard maps which can be used in decision making (Bonadonna et al., 2005; Macedonio et al., 2005; Folch and Sulpizio, 2010). These models rely on accurate parameterisations of ash sedimentation processes. However, it is often assumed that ash settles at its terminal fall velocity (Hazen, 1904), as determined from its size and the density contrast with the surrounding atmosphere (Clift and Gauvin, 1971; Ganser, 1993). Such a scheme predicts that the model grain size of deposited ash should decrease monotonically with distance from the vent (Bursik et al., 1992; Sparks et al., 1992). Deposits, however, sometimes record more complicated features such as bimodal size distributions whilst remotely sensed GSDs of the ash plume from the 2010 eruption of Eyjafjallajökull also showed that the effective ash radius did not monotonically decrease with distance from the vent (Bonadonna et al., 2011). Indeed, it is increasingly apparent that collective sedimentation processes can strongly control the sedimentation of ash. One commonly cited mechanism is ash aggregation, whereby ash particles stick together, increasing their effective size and thus their fall velocity (Carey and Sigurdsson, 1982; Sorem, 1982; Lane et al., 1993; Bonadonna et al., 2011; Brown et al., 2012). Another

possibility though is that collective sedimentation can occur through the occurrence of convective instabilities which drive larger scale fluid motions that can drive ash sedimentation through downward-propagating finger structures (Bonadonna et al., 2002, 2011; Carazzo and Jellinek, 2012; Manzella et al., 2015; Scollo et al., 2017). These arise due to the formation of a gravitationally unstable interfacial layer at the base of ash clouds, which has previously been called the particle boundary layer or PBL (Carazzo and Jellinek, 2012).

Despite recent progress in understanding how convective instabilities form and evolve, there remains a number of key unanswered questions. In particular, no consideration has been given to the role of background velocity shear, which will be present due to buoyant spreading of the cloud and/or wind drag (Johnson et al., 2015). In this study, we explore how the presence of shear at the base of volcanic clouds, due to buoyant spreading, can influence collective settling behaviour. In particular, we show that there is a regime where Kelvin-Helmholtz shear instabilities (von Helmholtz, 1868; Kelvin, 1871) can interact with settling-driven gravitational instabilities (Hoyal et al., 1999; Blanchette and Bush, 2005) to produce larger fingers that can enhance the sedimentation of fine ash.

1.1. Settling-driven gravitational instabilities

Settling-driven gravitational instabilities (SDGIs) can occur when a particle suspension is emplaced above a denser fluid (Hoyal et al., 1999; Blanchette and Bush, 2005). Although this initial configuration is stable (Figure 1a), as particles settle into the lower layer, they can form an interfacial layer which is denser than the underlying fluid (Figure 1b). This unstable layer has previously been called the particle boundary layer (PBL) (Carazzo and

Jellinek, 2012). Once this PBL reaches a critical thickness, it can destabilise and generate downward-propagating fingers (Hoyal et al., 1999). SDGIs are similar to double-diffusive instabilities, where instead of particle-settling, the motion of the density-controlling components is governed by diffusion (Stern, 1960). For the purposes of this study, we are interested in cases where the settling velocity of the particles V_s is sufficiently high that diffusion can be neglected and double-diffusive instabilities do not occur.

SDGIs are important in geological settings as the downward velocity of the generated fingers are greater than the settling velocities of individual particles. This creates the potential for enhancing the sedimentation rate from buoyant particle suspensions. Such a hypothesis was first put forward by Bradley (1965) to explain rapid sedimentation of sediment in eutrophic lakes (Nipkow, 1920). In recent years, the study of SDGIs has focussed on two applications: sedimentation from volcanic clouds (Carazzo and Jellinek, 2012; Manzella et al., 2015; Scollo et al., 2017); and sedimentation from hypopycnal currents (Chen, 1997; Parsons et al., 2001; Snyder and Hsu, 2011; Rouhnia and Strom, 2015, 2017; Jazi and Wells, 2016, 2019).

To allow a more quantitative description of SDGIs that can be applied to multiple applications, we let the fluid have a base density of ρ_0 . We then allow that the density of the fluid can be altered by a single component, such as a solute or temperature. Assuming only small changes to density, the fluid density can be parameterised as $\rho_f(\mathbf{x}, t) = \rho_0[1 + \alpha s(\mathbf{x}, t)]$ where s is the concentration of the solute or the temperature, and α is the corresponding expansivity. Furthermore, s is considered to be a function of space \mathbf{x} and time t . Meanwhile, the particle concentration is represented by $\phi(\mathbf{x}, t)$ and

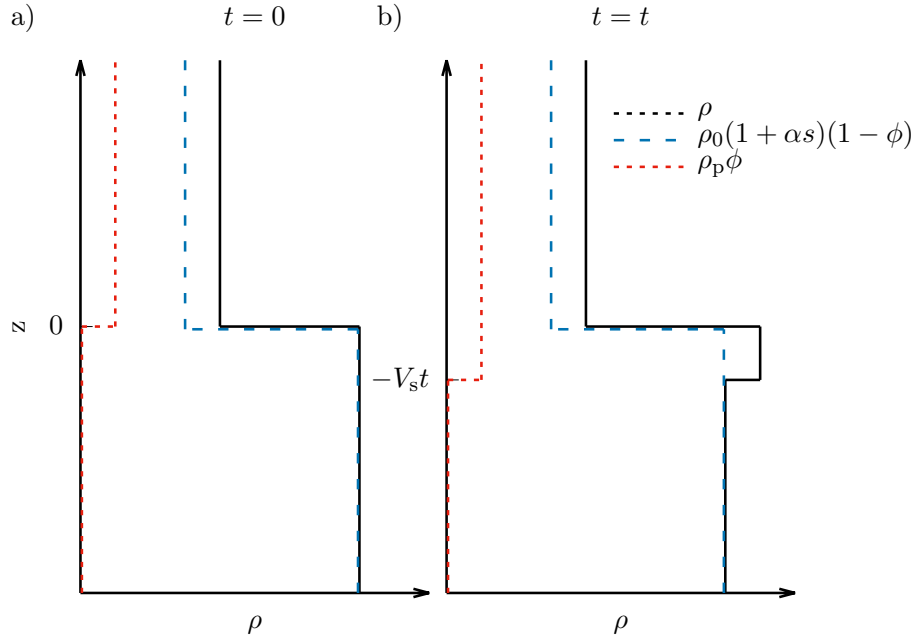


Figure 1: Sketch after Burns and Meiburg (2012) showing the formation mechanism of settling-driven gravitational instabilities. a) The initial configuration. The upper layer ($z > 0$) is a particle suspension of volume fraction ϕ in a fluid of density ρ_0 . The lower layer ($z < 0$) is a single-phase fluid but includes a density altering component (dissolved substance or temperature). Thus the density of the lower layer is given by $\rho_0(1+\alpha s)$ where α is the expansivity and s is the component concentration (or temperature). Throughout the tank, the blue and red lines represent the contributions of the fluid and particle phases, respectively, to the bulk density, which is given by the black line. b) The configuration after some time t . The front of the suspension has descended a distance $V_s t$ where V_s is the settling velocity of individual particles. This has generated an interfacial region with an unstable density configuration.

the density of the particle phase is ρ_p . Thus, the bulk density at any \mathbf{x} and t is given by

$$\rho(\mathbf{x}, t) = \rho_p \phi(\mathbf{x}, t) + \rho_0 [1 + \alpha s(\mathbf{x}, t)][1 - \phi(\mathbf{x}, t)]. \quad (1)$$

Considering the idealised situation presented in Figure 1, if the initial particle volume fraction of the upper layer is ϕ_0 and the initial solute concentration of the lower layer is s_0 , then, from equation 1, the densities of upper and lower layers, and the unstable PBL can be expressed as

$$\rho_u = \rho_p \phi_0 + \rho_0 (1 - \phi_0), \quad (2)$$

$$\rho_l = \rho_0 (1 + \alpha s_0), \quad (3)$$

and

$$\rho_{PBL} = \rho_p \phi_0 + \rho_0 (1 + \alpha s_0)(1 - \phi_0), \quad (4)$$

respectively. Since it is the interface between the PBL and the lower-layer that is unstable, the relevant choice of reduced gravity for the study of SDGIs is (Davies Wykes and Dalziel, 2014)

$$g'_{PBL} = \frac{2(\rho_{PBL} - \rho_l)g}{(\rho_{PBL} + \rho_l)} = 2Ag, \quad (5)$$

where $A = (\rho_{PBL} - \rho_l)/(\rho_{PBL} + \rho_l)$ is the Atwood number (Sharp, 1984).

Hoyal et al. (1999) developed two criteria for settling-driven instabilities to develop. The first arises from an analogy with thermal convection; defining δ to be the PBL thickness, a Grashof number $Gr = \frac{g'_{PBL}\delta^3}{\nu^2}$ (Turner, 1979), where ν is the kinematic viscosity of the fluid, can be defined as the ratio of buoyancy forces which act to destabilise the PBL and viscous forces which

resist this overturning. Therefore, Gr must exceed a critical value Gr_c , corresponding to a critical PBL thickness $\delta = \delta_c$, at which the PBL can detach and form fingers. By analogy with thermal convection, Hoyal et al. (1999) estimated that $Gr_c = 10^3$. The second criteria is that the individual settling velocity of the particles V_s must be less than the downward velocity of the generated fingers V_f ; otherwise particles will settle individually.

1.2. Stratified shear

Whilst many of the experimental and numerical studies of SDGIs have considered static configurations (Chen, 1997; Hoyal et al., 1999; Blanchette and Bush, 2005; Yu et al., 2014; Burns and Meiburg, 2015; Manzella et al., 2015; Rouhnia and Strom, 2015; Jazi and Wells, 2016; Scollo et al., 2017), both volcanic clouds and hypopycnal currents are examples of stratified shear flows, where there is a velocity gradient across a density interface. In fact, the effect of shear on SDGIs has not received extensive consideration. Some experimental studies have considered particle sedimentation from surface propagating gravity currents (Maxworthy, 1999; Parsons et al., 2001; McCool and Parsons, 2004; Sutherland et al., 2018; Jazi and Wells, 2019) whilst there has also been some theoretical treatment (Farenzena and Silvestri, 2017; Kondratenko et al., 2018). One question that remains to be addressed is for what conditions does shear enhance or inhibit sedimentation? It also remains to be understood how SDGIs can interact with shear instabilities. In stratified shear flows, three canonical instabilities can arise (Eaves and Balmforth, 2019): Kelvin-Helmholtz (KH) (von Helmholtz, 1868; Kelvin, 1871), Holmboe (Holmboe, 1962) and Taylor-Caulfield (TC) (Taylor, 1931; Caulfield et al., 1995). Of particular interest would be a predictive description of the flow

behaviour for different conditions and a parameterisation for the sedimentation rate.

1.3. Gravity currents

In this study, we generate shear between two density-stratified layers by allowing the upper layer to propagate as a buoyant gravity current, where the horizontal motion is generated by the difference in hydrostatic pressure in the two fluids. For an ideal, energy-conserving current, where mixing between the current and the ambient is negligible, the Froude number of the current is predicted to be (Benjamin, 1968)

$$Fr = \frac{U}{(g'H)^{1/2}} = \frac{1}{2}, \quad (6)$$

where U is the spreading velocity of the current, $g' = (\rho_l - \rho_u)g/\rho_l$ is the reduced gravity of the current, H is the depth of the total fluid volume and ρ_u is the density of the lower, ambient fluid.

2. Methods

Experiments were performed in a perspex flume of internal length 353 cm, width (12.2 ± 0.5) cm and depth 50 cm (Figure 2). The uncertainty on the width is due to bowing of the tank walls. During the experimental setup, two removable gates can be placed at 24 and 53 cm, respectively, from the left-hand end, creating three sections. The left-most section takes no part in the experiment, whilst the short middle section is where the particle suspension is prepared, and is referred to as the gated section (length 27 cm). The remaining length of the flume is called the environment (length 3m).

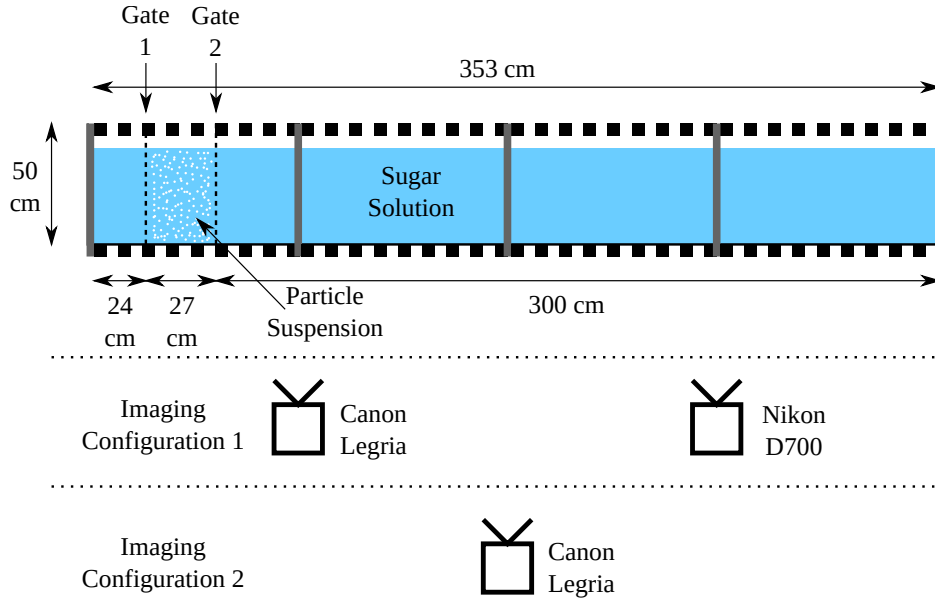


Figure 2: Sketch showing the experimental setup. The flume is separated into three section separated by two gates. The leftmost section is not involved in the experiment. The rightmost section is a sugar solution of constant density whereas the section between gates 1 and 2 is a mixture of fresh water and ballotini. The concentration of particles is varied between experiments. The experiment is initiated by removing gate 2. Experiments were imaged using one of two configurations.

The flume sits within a metal framework. Three vertical supports, each 3cm thick, at distances of 87 cm, 173.5 cm and 260 cm from the left-hand end prevent bowing. This effectively separates the flume into four, nearly equal, section. Behind each section a backing board is placed. For experiments with no particles, red or blue food colouring is added to the current and the backing board is white. Otherwise the boards are black. The top 5 cm of each board is a row of (5×5) cm^2 squares, alternating in colour from black-to-white. Meanwhile, at the base of the tank, tape is used to create a similar scale.

The day before an experiment, the flume is filled up to a depth of 47.5 cm. Separately, the desired mass of sugar is completely dissolved in approximately 15 l of water. The flume and sugar solution are then both allowed to equilibrate to room temperature overnight. The next day, the flume is imaged (single frame) in its current configuration. In some experiments, the whole flume was imaged using a Canon Legria HFG40. In others, this camera was position closer to the tank, but only imaged the left-hand half of the flume, whilst the right-hand half was imaged using a Nikon D700 (DSLR). The captured frame(s) are used as reference images using the top(back) and bottom(front) scales. By capturing the image with the back scale partially submerged, it is possible to correct position measurements for distortion due to the refractive index (RI) of the water.

The flume water level is then lowered until it is of a depth of approximately 36.5 cm. Gates 1 and 2 are then put in place. The sugar solution is then added to the environment section. The gated section is then topped up with water until the water depth there is the same as the environment. This procedure results in a water depth of approximately 40 cm. The environment section is rigorously stirred. The RI of fluid from four positions in the environment section (top and bottom, near and far from the gate) is measured using a refractometer to ensure a uniform density. The RI of the gated section is also measured to check that there has been no significant leakage of sugar solution through the gate. A calibrated digital thermometer is used to measure the temperature of both sections. In all experiments, the maximum difference in temperature between the sections was 0.1 °C.

Recording of the experiment then begins. The required mass of particles

is added to the gated section which is thoroughly stirred to ensure a uniform particle concentration. Finally, gate 2 is removed and the particle suspension spreads along the free surface as a buoyant gravity current. Once the current head reaches the end of the tank, gate 2 is returned to its position and recording stops.

The particles used were glass spheres with a density of $(2.519 \pm ??)$ g cm $^{-3}$, as measured by helium pycnometry using an Ultrapyc 1200e. They had a unimodal size distribution centred on a mode of 36 μm and a standard deviation of 12 μm , as determined from static light scattering using a Bettersizer S3 Plus. Figure 3 shows the measured size distribution of the particles.

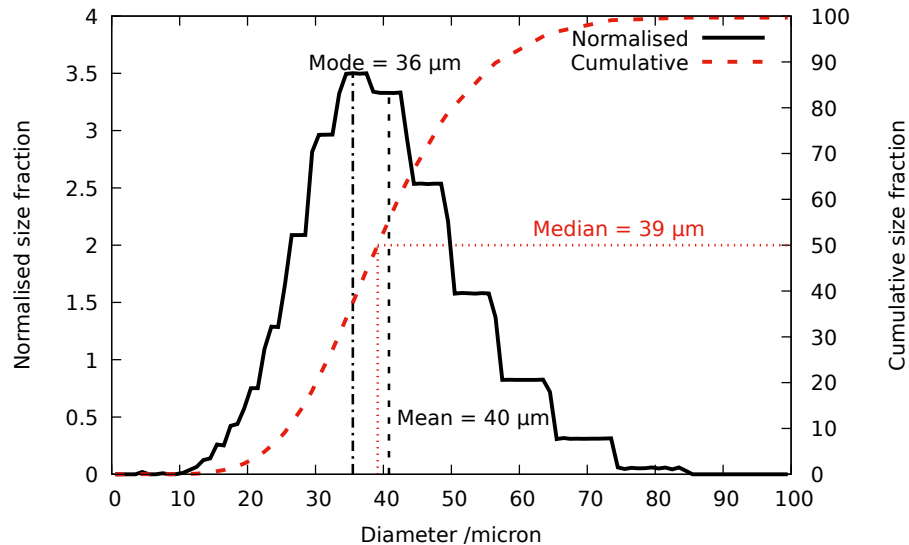


Figure 3: Normalised and cumulative volume-weighted size distributions of the particles used in the experiments.

3. Results

3.1. Currents without particles

Figure 4 shows the evolution of the current in experiment GC3.

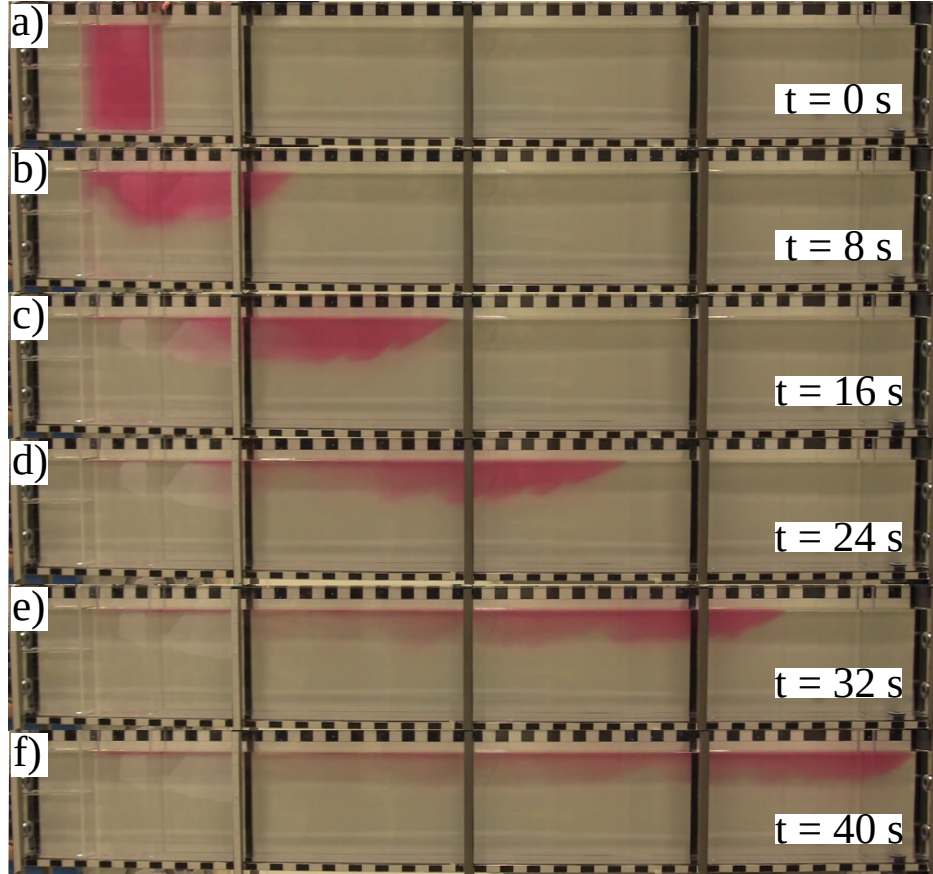


Figure 4: Sequence of images showing experiment GC3 ($\phi = 0$, $g\tau = 0.162 \text{ m s}^{-2}$).

Figure 5 shows the evolution of the current in experiment GC9.

3.2. Particle-bearing currents

Figure 6 shows the evolution of the current in experiment GC42.



Figure 5: Sequence of images showing experiment GC9 ($\phi = 0$, $g\tau = 0.563 \text{ m s}^{-2}$).

Figure 7 shows the evolution of the current in experiment GC48.

Figure 8 shows the evolution of the current in experiment GC45.



Figure 6: Sequence of images showing experiment GC42.

4. Discussion

5. Conclusions

Acknowledgements

References

Anderson, J.O., Thundiyil, J.G., Stolback, A., 2012. Clearing the air: A review of the Effects of Particulate Matter Air Pollution on Human Health. J. Med. Toxicol. 8, 166–175.

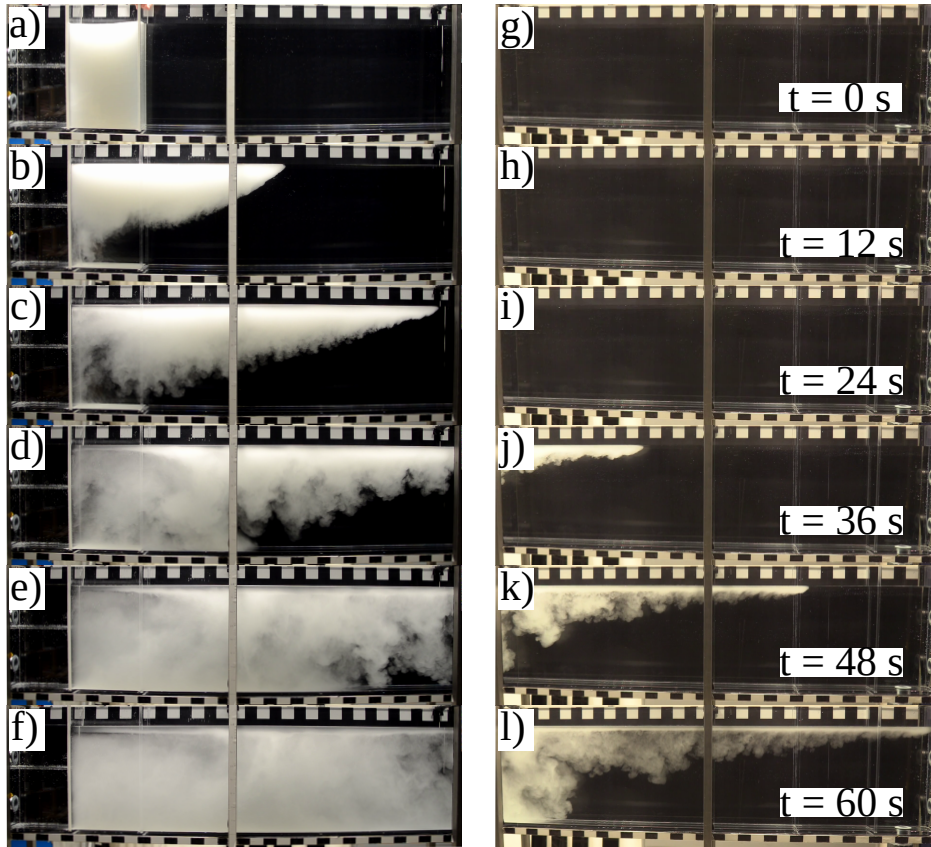


Figure 7: Sequence of images showing experiment GC48. a-f) show the left hand side of the tank whilst g-l) show the right hand side.

Baxter, P.J., Horwell, C.J., 2015. Impacts of Eruptions on Human Health, in: H. Sigurdsson (Ed.), The Encyclopedia of Volcanoes. Elsevier Inc., pp. 1035–1047.

Benjamin, T.B., 1968. Gravity currents and related phenomena. J. Fluid Mech. 31, 209–248.

Blanchette, F., Bush, J.W.M., 2005. Particle concentration evolution and

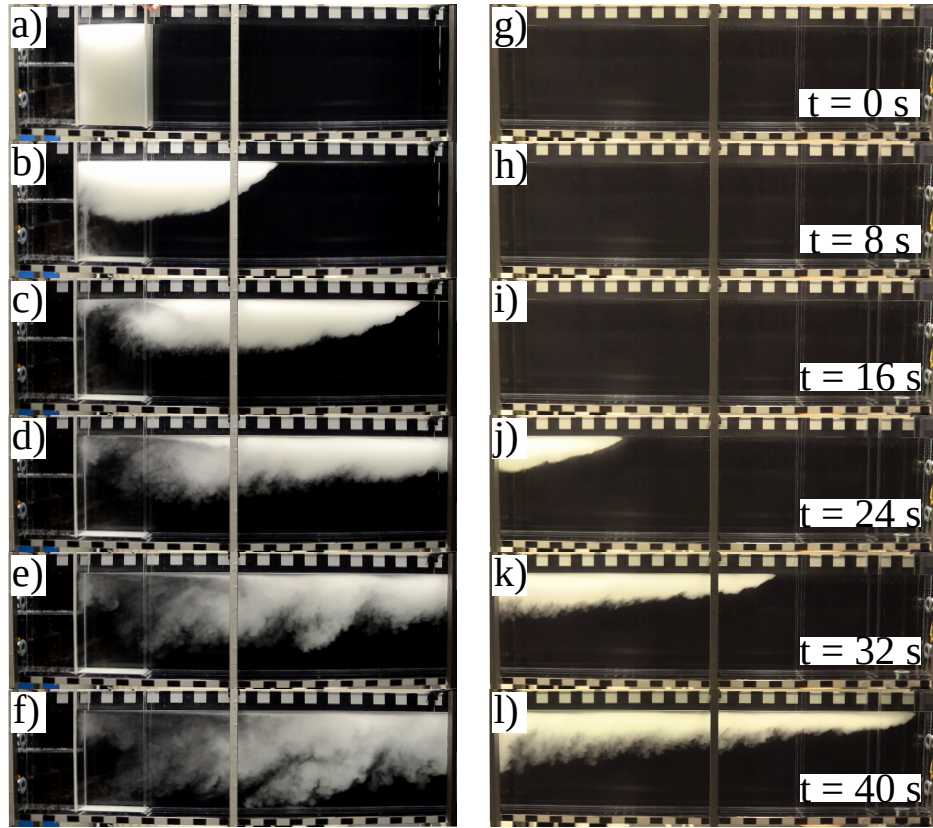


Figure 8: Sequence of images showing experiment GC45. a-f) show the left hand side of the tank whilst g-l) show the right hand side.

sedimentation-induced instabilities in a stably stratified environment. Phys. Fluids 17, 073302.

Bonadonna, C., Connor, C.B., Houghton, B.F., Connor, L., Byrne, M., Laing, A., Hinks, T.K., 2005. Probabilistic modeling of tephra dispersal: Hazard assessment of a multiphase rhyolitic eruption at Tarawera, New Zealand. J. Geophys. Res. Solid Earth 110.

Bonadonna, C., Folch, A., Loughlin, S., Puempel, H., 2012. Future develop-

ments in modelling and monitoring of volcanic ash clouds: outcomes from the first IAVCEI-WMO workshop on Ash Dispersal Forecast and Civil Aviation. *Bull. Volcanol.* 74, 1–10.

Bonadonna, C., Genco, R., Gouhier, M., Pistolesi, M., Cioni, R., Alfano, F., Hoskuldsson, A., Ripepe, M., 2011. Tephra sedimentation during the 2010 Eyjafjallajökul eruption (Iceland) from deposit, radar, and satellite observations. *J. Geophys. Res. Solid Earth* 116.

Bonadonna, C., Mayberry, G.C., Calder, E.S., Sparks, R.S.J., Choux, C., Jackson, P., Lejeune, A.M., Loughlin, S.C., Norton, G.E., Rose, W.I., Ryan, G., Young, S.R., 2002. Tephra fallout in the eruption of Soufrière Hills Volcano, Montserrat. *Geol. Soc. Lond. Mem.* 21, 483–516.

Bradley, W.H., 1965. Vertical Density Currents. *Science* 150, 1423–1428.

Brown, R.J., Bonadonna, C., Durant, A.J., 2012. A review of volcanic ash aggregation. *Phys. Chem. Earth* 45–46, 65–78.

Budd, L., Griggs, S., Howarth, D., Ison, S., 2011. A Fiasco of Volcanic Proportions? Eyjafjallajökull and the Closure of European Airspace. *Mobilities* 6, 31–40.

Burns, P., Meiburg, E., 2012. Sediment-laden fresh water above salt water: linear stability analysis. *J. Fluid Mech.* 691, 279–314.

Burns, P., Meiburg, E., 2015. Sediment-laden fresh water above salt water: nonlinear simulations. *J. Fluid Mech.* 762, 156–195.

- Bursik, M.I., Sparks, R.S.J., Gilbert, J.S., Carey, S.N., 1992. Sedimentation of tephra by volcanic plumes: I. Theory and its comparison with a study of the Fogo A plinian deposit, São Miguel (Azores). *Bull. Volcanol.* 54, 329–344.
- Carazzo, G., Jellinek, A.M., 2012. A new view on the dynamics, stability and longevity of volcanic clouds. *Earth Planet. Sci. Lett.* 325–326, 39–51.
- Carey, S.N., Sigurdsson, H., 1982. Influence of particle aggregation on deposition of distal tephra from the May 18, 1980, eruption of Mt. St. Helens volcano. *J. Geophys. Res. Solid Earth* 87, 7061–7072.
- Caulfield, C.P., Peltier, W.R., Yoshida, W.R., Ohtani, M., 1995. An experimental investigation of the instability of a shear flow with multilayered density stratification. *Phys. Fluids* 7, 3028–3041.
- Chen, C.F., 1997. Particle flux through sediment fingers. *Deep-Sea Res. PT.* 1 44, 1645–1654.
- Clift, R., Gauvin, W.H., 1971. Motion of entrained particles in gas streams. *Can. J. Chem. Eng.* 49, 439–448.
- Cook, R.J., Baron, J.C., Papendick, R.I., III, G.J.W., 1981. Impact on Agriculture of the Mount St. Helens Eruptions. *Science* 211, 16–22.
- Craig, H., Wilson, T., Stewart, C., Outes, V., Villarosa, G., Baxter, P., 2016. Impacts to agriculture and critical infrastructure in Argentina after ashfall from the 2011 eruption of the Cordón Caulle volcanic complex: an assessment of published damage and function thresholds. *J. Appl. Volcanol.* 5, 7.

- Cronin, S.J., Headley, M.J., Neall, V.E., Smith, R.G., 1998. Agronomic impact of tephra fallout from the 1995 and 1996 Ruapehu Volcano eruptions, New Zealand. *Environ. Geol.* 34, 21–30.
- Davies Wykes, M.S., Dalziel, S.B., 2014. Efficient mixing in stratified flows: experimental study of a Rayleigh-Taylor unstable interface within an otherwise stable stratification. *J. Fluid Mech.* 756, 1027–1057.
- Eaves, T.S., Balmforth, N.J., 2019. Instability of sheared density interfaces. *J. Fluid Mech.* 860, 145–171.
- Elisondo, M., Baumann, V., Bonadonna, C., Pistolesi, M., Cioni, R., Bertagnini, A., Biass, S., Herrero, J., Gonzalez, R., 2016. Chronology and impact of the 2011 Cordón Caulle eruption, Chile. *Nat. Hazards Earth Syst. Sci.* 16, 675–704.
- Farenzena, B.A., Silvestri, J.H., 2017. Linear stability analysis of particle-laden hypopycnal plumes. *Phys. Fluids* 29, 124102.
- Folch, A., 2012. A review of tephra transport and dispersal models: Evolution, current status, and future perspectives. *J. Volcanol. Geotherm. Res.* 235-236, 96–115.
- Folch, A., Sulpizio, R., 2010. Evaluating long range-range volcanic ash hazard using supercomputing facilities: application to the Somma-Vesuvius (Italy), and consequences for civil aviation over the Central Mediterranean Area. *Bull. Volcanol.* 72, 1039–1059.
- Ganser, G.H., 1993. A rational approach to drag prediction of spherical and nonspherical particles. *Powder Technol.* 77, 143–152.

- Hazen, A., 1904. On sedimentation. *Trans. Am. Soc. Civ. Eng.* 53, 45–88.
- von Helmholtz, H., 1868. Über discontinuierliche Flüssigkeits-Bewegungen. *Akademie der Wissenschaften zu Berlin.*
- Holmboe, J., 1962. On the behaviour of symmetric waves in stratified shear layers. *Geophys. Publ.* 24, 67–113.
- Hoyal, D.C.J.D., Bursik, M.I., Atkinson, J.F., 1999. Settling driven convection: A mechanism of sedimentation from stratified fluids. *J. Geophys. Res. Oceans* 104, 7953–7966.
- Jazi, S.D., Wells, M.G., 2016. Enhanced sedimentation beneath particle-laden flows in lakes and the ocean due to double-diffusive convection. *Geophys. Res. Lett.* 43, 10883–10890.
- Jazi, S.D., Wells, M.G., 2019. Dynamics of settling-driven convection beneath a sediment-ladenbuoyant overflow: Implications for the length-scale of deposition in lakes and the coastal ocean. *Sedimentology* 67, 699–720.
- Johnson, C.G., Hogg, A.J., Huppert, H.E., Sparks, R.S.J., Phillips, J.C., Slim, A.C., Woodhouse, M.J., 2015. Modelling intrusions through quiescent and moving ambients. *J. Fluid Mech.* 771, 370–406.
- Kampa, M., Castanas, E., 2007. Human health effects of air pollution. *Environ. Pollut.* 151, 362–367.
- Kelvin, W., 1871. The influence of wind on waves in water supposed frictionless. *Phil. Mag.* 42, 368–374.

- Konopliv, N., Lesshafft, L., Meiburg, E., 2018. The influence of shear on double-diffusive and settling-driven instabilities. *J. Fluid Mech.* 849, 902–926.
- Lane, S.J., Gilbert, J.S., Hilton, M., 1993. The aerodynamic behaviour of volcanic aggregates. *Bull. Volcanol.* 55, 481–488.
- Macedonio, G., Costa, A., Longo, A., 2005. A computer model for volcanic ash fallout and assessment of subsequent hazard. *Comput. Geosci.* 31, 837–845.
- Manzella, I., Bonadonna, C., Phillips, J.C., Monnard, H., 2015. The role of gravitational instabilities in deposition of volcanic ash. *Geology* 43, 211–214.
- Maxworthy, T., 1999. The dynamics of sedimenting surface gravity currents. *J. Fluid Mech.* 392, 27–44.
- McCool, W.M., Parsons, J.D., 2004. Sedimentation from buoyant fine-grained suspensions. *Cont. Shelf Res.* 24, 1129–1142.
- Nipkow, F., 1920. Vorläufige Mitteilungen über Untersuchungen des Schlammabsatzes im Zürichsee. *Z. Hydrol.* 1, 100–122.
- Parsons, J.D., Bush, J.W.M., Syvitski, J.P.M., 2001. Hyperpycnal plume formation from riverine outflows with small sediment concentrations. *Sedimentology* 48, 465–478.
- Rouhnia, M., Strom, K., 2015. Sedimentation from flocculated suspensions

- in the presence of settling-driven gravitational interface instabilities. *J. Geophys. Res. Oceans* 120, 6384–6404.
- Rouhnia, M., Strom, K., 2017. Sedimentation from buoyant muddy plumes in the presence of turbulent mixing: An experimental study. *J. Geophys. Res. Oceans* 122, 2652–2670.
- Scollo, S., Bonadonna, C., Manzella, I., 2017. Settling-driven gravitational instabilities associated with volcanic clouds: new insights from experimental investigations. *Bull. Volcanol.* 79, 39.
- Scollo, S., Prestifilippo, M., Spata, G., D'Agostino, M., Coltelli, M., 2009. Monitoring and forecasting Etna volcanic plumes. *Nat. Hazards Earth Syst. Sci.* 9, 1573–1585.
- Sharp, D.H., 1984. An overview of the Rayleigh-Taylor instability. *Physica D* 12, 3–18.
- Snyder, P.J., Hsu, T., 2011. A numerical investigation of convective sedimentation. *J. Geophys. Res. Oceans* 116, C09024.
- Sorem, R.K., 1982. Volcanic ash clusters: Tephra rafts and scavengers. *J. Volcanol. Geotherm. Res.* 13, 63–71.
- Sparks, R.S.J., Bursik, M.I., Ablay, G.J., Thomas, R.M.E., Carey, S.N., 1992. Sedimentation of tephra by volcanic plumes. Part 2: controls on thickness and grain-size variations of tephra fall deposits. *Bull. Volcanol.* 54, 685–695.

- Stern, M.E., 1960. The "Salt-Fountain" and Thermohaline Convection. *Tellus* 12, 172–175.
- Sutherland, B.R., Gingras, M.K., Knudsen, C., Steverango, L., Surna, C., 2018. Particle-bearing currents in uniform density and two-layer fluids. *Phys. Rev. Fluids* 3, 023801.
- Taylor, G.I., 1931. Effect of variation in density on the stability of superposed streams of fluid. *Proc. R. Soc. Lond.* 132, 449–523.
- Turner, J.S., 1979. Buoyancy effects in fluids. Cambridge Univ. Press.
- Webster, H.N., Thomson, D.J., Johnson, B.T., Heard, I.P.C., Turnbull, K., Marendo, F., Kristiansen, N.I., Dorsey, J., Minikin, A., Weinzierl, B., Schumann, U., R. S, J.S., Loughlin, S.C., Hort, M.C., Leadbetter, S.J., Devenish, B.J., Manning, A.J., Witham, C.S., Haywood, J.M., Golding, B.W., 2012. Operational prediction of ash concentrations in the distal volcanic cloud from the 2010 Eyjafjallajökull eruption. *J. Geophys. Res. Atmos.* 117.
- WHO, 2013. Health effects of particulate matter. Technical Report. World Health Organisation.
- Wilson, G., Wilson, T.M., Delinge, N.I., Cole, J.W., 2014. Volcanic hazard impacts to critical infrastructure: A review. *J. Volcanol. Geotherm. Res.* 286, 148–182.
- Wilson, T., Cole, J., Cronin, S., Stewart, C., Johnston, D., 2011. Impacts on agriculture following the 1991 eruption of Volcan Hudson, Patagonia, lessons for recovery. *Nat. Hazards* 57, 185–212.

Witham, C.S., Hort, M.C., Potts, R., Servanckx, R., Husson, P., Bonnardot, F., 2007. Comparison of the VAAC atmospheric dispersal models using the 1 November 2004 Grimsvötn eruption. *Meteorol. Appl.* 14, 127–38.

Yu, X., Hsu, T., Balachandar, S., 2014. Convective instability in sedimentation: 3-D numerical study. *J. Geophys. Res. Oceans* 119, 8141–8161.